

Daily reference evapotranspiration for California using satellite imagery and weather station measurement interpolation

Quinn Hart ^{a,*} Marcela Brugnach ^{a,1} Bekele Temesgen ^b

Carlos Rueda ^a Susan Ustin ^a Kent Frame ^b

^a *CalSpace, University of California, Davis, Davis, CA, USA*

^b *California Irrigation Management Information System (CIMIS), California*

Department of Water Resources, Sacramento, CA, USA

Abstract

Spatially distributed ET_0 is calculated to produce daily ET_0 maps for the State of California at high spatial resolution, $(2\text{ km})^2$. Hourly NOAA GOES visible channel imager data are used to modify modeled radiation estimates. These are combined with interpolated California Irrigation Management Information System (CIMIS) weather station meteorological data to satisfy the Penman-Monteith ET_0 equation. Data have been acquired and ET_0 estimated daily from February 2003 through April 2006.

Key words: evapotranspiration, Penman-Monteith equation, satellite imaging, remote sensing

PACS: 92.40.Zg, 92.40.Je, 42.68.Wt

[Table 1 about here.]

1 Introduction

California experiences periodic water shortages from natural climate variability, e.g., El Niño cycles, and is at risk for potential longer-term extended droughts due to climate change. Winters with below normal snowpack, either from low precipitation or early snowmelt, cause low summer streamflow and inadequate water supplies for agriculture and urban uses. California agriculture is a \$25 billion/year economic sector and the economy is at risk without efficient water management. Improved monitoring can increase the efficiency of water use and mitigate potential losses.

The CIMIS program was successfully introduced by the California Department of Water Resource and the University of California, Davis in 1982, to help farmers, turf managers and other resource managers develop water budgets that improve irrigation scheduling and limit over-watering. The CIMIS system is a repository of meteorological data collected at over 130 computerized weather stations located at key agricultural and municipal sites throughout California which provide comprehensive, timely, weather data collected hourly

* Corresponding author.

Email addresses: qjhart@ucdavis.edu (Quinn Hart), mbrugnac@usf.us (Marcela Brugnach), temesgen@water.ca.gov (Bekele Temesgen), carueda@ucdavis.edu (Carlos Rueda), sustin@ucdavis.edu (Susan Ustin), kframe@water.ca.gov (Kent Frame).

¹ Currently: Institute of Environmental Systems Research, University of Osnabrueck, Germany

and daily.

This paper builds on the CIMIS base by developing a methodology to extend the weather station data to spatial daily ET_0 maps of California. Daily reference ET_0 maps for California are calculated for a high spatial resolution (2 km) 2 grid. We developed daily statewide monitoring capability for estimating reference evapotranspiration ET_0 using the National Oceanic and Atmospheric Administration (NOAA) Geostationary Operational Environmental Satellite (GOES) data and ground based weather data from the CIMIS weather stations. Figure 1 shows an example ET_0 map for California.

[Fig. 1 about here.]

Evapotranspiration (ET) is a measure of the water requirements for the healthy functioning of a particular plant-soil-atmosphere system. By knowing the water requirements of a particular system, a variety of water issues, such as irrigation scheduling and design, landscape planning and water transfer can be addressed.

By specifying standard crop parameters with a well irrigated system, a standard ET_0 can be determined that requires only meteorological measurements. A standardized ET_0 separates atmospheric drivers on ET from crop specifics, and reduces the need to develop more complex models for specific crop types and growth stages. Generally, field specific ET s are developed as simple linear relationships to ET_0 .

The American Society of Civil Engineers (ASCE) Evapotranspiration in Irrigation and Hydrology Committee (ASCE-ET) defines one standardized reference evapotranspiration equation and two reference surfaces (Walter et al.,

2000). The reference equation is:

$$ET_0 = \frac{0.408\Delta(R_n - G) + \gamma \frac{C_n}{T+273}(e_s - e_a)}{\Delta + \gamma(1 + \frac{C_d}{U_2})} \quad (1)$$

This paper uses the hypothetical short crop surface for ET_0 , which resembles an extensive surface of green grass of uniform height, actively growing with adequate water and a canopy completely shading the ground. The reference crop has an assumed height of 0.12 m, daily r_s of 70 sm^{-1} , and coefficients, $C_n = 900$ and $C_d = 0.34$.

The ASCE-ET equation describes the control that environmental factors, such as solar radiation, wind speed, air temperature and humidity exert on ET_0 . These factors influence ET either by providing the energy for vaporization or by increasing efficiency in the removal of water vapor from the surface.

The following equations describe the parameters in the ET_0 equation in more detail:

$$ET_0 = \frac{0.408\Delta(R_n - G) + \gamma \frac{900}{T_m+273} U_2(e_s - e_a)}{\Delta + \gamma(1 + 0.34U_2)} \quad (2)$$

$$R_n = R_{ns} - R_{nl} \quad (3)$$

$$R_{ns} = (1 - \alpha)R_s \quad (4)$$

$$R_s = KR_{so} \quad (5)$$

$$R_{nl} = (1.35 \frac{R_s}{R_{so}} - 0.35)(0.34 - 0.14\sqrt{ea})\sigma \frac{T_n^4 + T_x^4}{2} \quad (6)$$

$$\Delta = \frac{4099e_a}{(T_m + 237.3)^2} \quad (7)$$

$$\gamma = 0.665e-3(101.3 \frac{293 - 0.0065z^{5.26}}{293}) \quad (8)$$

$$T_m = \frac{T_n + T_x}{2} \quad (9)$$

$$e_s = \frac{0.6108}{2} \left(\exp \left(\frac{17.27T_n}{T_n + 237.3} \right) + \exp \left(\frac{17.27T_x}{T_x + 237.3} \right) \right) \quad (10)$$

$$e_a = 0.6108 \exp \left(\frac{17.27T_{dewp}}{T_{dewp} + 237.3} \right) \quad (11)$$

$R_n - G$ represents the supply of energy available to vaporize water. For daily calculations, net radiation, R_n , is dominant and soil heat flux density, G , is assumed to be negligible. R_n is calculated as the difference between the incoming net shortwave radiation, R_{ns} and the outgoing net longwave radiation, R_{nl} , (Eq. 3). R_{ns} represents the portion of R_s that is not reflected (Eq. 5), where R_s , is the amount of incoming solar radiation that reaches the earth surface after accounting for the effects of absorption, scattering and reflection of the atmosphere. R_s is modeled as a fraction of R_{so} , where K is determined from GOES satellite data, more fully described in Section 2.2. The reference crop has an albedo of 0.23. Net longwave radiation, R_{nl} represents the exchange of radiation between the crop surface and the atmosphere and clouds (Eq. 6).

In the ET_0 equation, the water content of the air is represented with $(e_s - e_a)$

expressing the vapor pressure deficit. Saturation vapor pressure, e_s , is computed as the mean between saturation vapor pressure at maximum air temperature and saturation vapor pressure at minimum air temperature (Eq. 10). The actual vapor pressure, e_a is calculated as a function of dew point temperature (Eq. 11). The slope of the vapor pressure-temperature curve is Δ (Eq. 7) and γ is the psychrometric constant. T_m is the mean air temperature (Eq. 9).

2 ET_0 Parameter Estimation

Calculating ET_0 requires meteorological data including; air temperature, incoming solar radiation, average daily wind speed and dew point temperature. Solar radiation is derived from models coupled with GOES satellite imagery for cloud cover estimation. Temperatures, wind speed and dew point are derived by interpolating point data from the network of CIMIS weather stations.

For spatial estimates of ET_0 , the parameters need to be calculated for every pixel in a gridded surface of California. Figure 2 shows an overview of all steps for calculating statewide ET_0 . These steps include procedures for spatially interpolating CIMIS data as well as processing GOES image data to predict the clear sky factor and the resultant solar radiation. All processing steps are performed using existing or created modules in the Geographic Resources Analysis Support System (GRASS) (GRASS Development Team, 2006; Neteler and Mitasova, 2004) Geographic Information System (GIS) application.

[Fig. 2 about here.]

Figure 2, shows two separate methods were used to calculate temperature related parameters, discussed in Section 2.1. This small ensemble of estimates

gives a measure of potential errors in the estimates, and are used in a sensitivity analysis of the results, discussed in Section 3.

2.1 *Ground Station Data Interpolation*

Maximum air temperature, T_x , minimum air temperature, T_n , dew point, T_{dewp} , and average wind speed, U_2 , are derived by spatially interpolating point data from the CIMIS network. These weather stations are spatially distributed as shown in Figure 3. Areas such as California’s central valley have a dense distribution of stations, but mountainous, urban, and desert regions are less represented. This distribution results from the design to inform California’s agricultural irrigation practices. For various reasons, not all stations report data daily; on average it is possible to use data from about 120 stations. Figure 3 groups stations by elevation with higher stations having larger symbols. Figure 3 also identifies three small transects used to validate temperature lapse rates.

[Fig. 3 about here.]

Spatial interpolation generates surfaces of continuous fields from data collected at discrete locations. Interpolation methods are built on assumptions that attributes are continuous over space and values close together are more similar than those farther apart.

Several interpolation methods were investigated. Criteria for method selection included accuracy of results, code availability, and computational efficiency. Multiple interpolations created a small ensemble of predictions that allowed for an estimation of errors. After investigating several methods, we used Regular-

ized Spline with Tension (RST) and Truncated Gaussian (TG) interpolations.

The TG, sometimes identified as DayMet (Peter E. Thornton and White, 1997) method refers to an interpolation method that generates daily surfaces of temperature, humidity and other variables over large regions of complex terrain. The method applies the spatial convolution of a Gaussian filter with a set of observations. The weight $W_{t,\alpha}(r)$ given to an observation with a radial distance r from the center of the filter is given by $W_{t,\alpha}(r) = \exp(-(r/t)^2\alpha) - \exp(-\alpha)$. The parameter t determines a truncation distance such that the weight is zero if $r > t$. The parameter α adjusts the shape of the filter.

On a daily basis, we determine these parameters by exhaustively searching the parameter space and selecting the values that minimize the estimation error using the standard leave-one-out cross-validation methodology. The TG method estimates the truncation radius via an iterative algorithm such that it is decreased for regions with high observation density and increased otherwise. Elevation data are included in the method as a post-correction step. In the case of temperature, this is performed by weighted least-square regression.

Although the TG method is applied as an inverse-distance algorithm, the Gaussian function does not force the resultant surface to pass through the observations, thus allowing for smoother surfaces.

RST (Mitasova et al., 1995; Neteler and Mitasova, 2004) is a method that simulates passing a flexible plate close to the known data points while minimizing the energy to bend the plate. Two parameters drive the shape of the interpolation. The tension parameter tunes the plate from stiff to flexible. Low tension (stiff) plates are smoother, but can miss high gradient changes. High tension (flexible) plates are less smooth and allow higher gradient changes about indi-

vidual points. Tension also controls the influence of neighboring points. Lower tension gives points influence over longer distances.

The smoothing parameter controls how much the fitted surface can deviate from the measured point values. Since the spatial interpolation assigns one value for each $(2 \text{ km})^2$ pixel, variation of the RST from the measured points is allowed.

Both 2-dimensional and 3-dimensional splines with elevation were used. 2-D RSTs interpolations along with lapse rate normalization were made for temperature estimations. Wind speed estimations used 3-D splines. Parameter values were selected through cross-validation exercises in conjunction with visual inspection and were kept constant for all estimates.

One example of how the location of CIMIS stations is not representative of California is the distribution of stations as a function of elevation. Figure 4 shows the difference in the distribution and range of the elevation, comparing the CIMIS stations and California as a whole. The station elevations under-represent the higher elevations in California. Because of this, extrapolating temperature measurements from CIMIS stations to regions with differing elevations is error prone.

[Fig. 4 about here.]

The RST interpolation uses a simple lapse rate to normalize the temperatures from all stations to a standard elevation. The measurements were normalized to sea level using a standard lapse rate of $5 \text{ }^{\circ}\text{C}/\text{km}$. A 2-D spline interpolation was fit to the normalized data. The parameters to the RST, were chosen with low tension and high smoothness resulting in a smooth interpolation over

the normalized data. The resulting values were then re-corrected by lapse rate along with elevation data for the state. Figure 5 shows an example for temperatures calculated using this method.

[Fig. 5 about here.]

A lapse rate of $5^{\circ}\text{C}/\text{km}$ was chosen for all temperature interpolations, T_x, T_n , and T_{dewp} . An examination of measured lapse rates between close stations, shows lapse rates for California vary widely. Figure 3 shows three regions, labeled Sacramento, South Valley, and South Coast, with some moderate elevation differences between proximate stations. To test the lapse rate within these regions, the difference in temperature versus the difference in elevation was calculated for all pairs of stations within each region, for each day in the three year time window. Figure 6 shows these relationships and the calculated lapse rates for each region and temperature interpolation. The lapse rates vary widely between regions, with only T_{dewp} showing any statewide stability.

[Fig. 6 about here.]

Including seasonal differences compounds this confusion. Table 2 shows lapse rates for these regions averaged at monthly intervals. In addition to regional differences, time-dependant changes in lapse rate are apparent. While it is fairly easy to explain aspects of these results (for example, the diminishing effect of maritime influences in the South Coast region causing an inversion of lapse rates moving inland with higher elevations) it is clear that simple interpolations over a complex landscape can be only partially successful.

[Table 2 about here.]

Final temperature estimates were generated by averaging the results of TG and RST interpolations. Figure 7 shows a comparison of the two methods for a single day.

[Fig. 7 about here.]

Average daily wind speed measured at 2m height above the surface is used to compute the aerodynamic resistance, which represents a resistance to diffusion that air above the vegetative surface imposes on ET . Average wind speed maps were generated using 3D RST. Figure 8 shows some example wind speed interpolations. For these estimates, more flexible surfaces were fit. High winds reported from single stations cause anomalous effects in the interpolation around those points. Another problem with wind speed interpolations is that only the speed and not wind direction is included in the interpolation model.

[Fig. 8 about here.]

2.2 Radiation Models

Radiative inputs to the ASCE-ET equation include the energy terms; R_s and R_{nl} . Solar radiation can be measured directly or modeled. Longwave radiation is primarily a function of surface temperature, but is also affected by the daily average cloud cover and water vapor which affect the emissivity.

2.2.1 Solar Radiation, R_s

Solar radiation is a linear term in the ET_0 equation and in most cases in California is the driving factor in its calculation. Therefore it is important to measure this parameter accurately. CIMIS stations measure solar radiation directly, but this parameter cannot be reliably interpolated spatially, since it is dependant on the daily cloud cover, which does not interpolate well from station data points.

The method for the calculation of R_s combines model predictions of clear sky radiation with hourly estimates of cloud cover using GOES visible channel imager data. This method for estimating solar radiation is independent of measurements at the CIMIS stations. The clear sky solar radiation model used is Heliosat-II (Rigollier et al., 2000; Leferve et al., 2002).

For each location in California, the sunrise and sunset times are calculated each day. Within the sunlit period, GOES data are available for each hour, as shown in Figure 9. The solar zenith angle for each hour are shown with solid lines. From each of these hourly GOES images, a clear sky factor is calculated (Section 2.2.2). This factor is assumed constant over the intervals of time/sun angle shown with dotted lines. Clear sky radiation is calculated for each of these intervals. The clear sky radiation and clear sky factor are used to predict the actual radiation for each interval. Finally, the contributions from all intervals are summed for the daily estimate of solar radiation.

[Fig. 9 about here.]

The Heliosat-II model uses an analytical integration over solar angles and it is simple to change the frequency of the GOES cloud cover estimates. Missing

cloud cover estimates, caused by lost GOES images, are handled by extending the intervals adjacent to the missing times. The analytical integration assigns appropriate weights to the remaining cloud cover estimates.

Atmospheric transmission in the Heliosat-II model combines aspects of aerosols, relative humidity, ozone, and molecular scattering into a single parameter, the Linke turbidity, which relates the optical depth for an arbitrary atmosphere to an equivalent atmospheric depth of a Rayleigh-only scattering atmosphere. Along with the sun's geometry and the elevation, the predicted radiation is calculated with this parameter. Seasonal values of the Linke turbidity are derived from a world database of turbidity estimates (Remund et al., 2003).

The percent difference in Heliosat-II compared to simpler solar radiation models such as that found in the FAO *ET* guidelines (Allen et al., 1998) range from -20% to +6%, though is generally about 6% less than the FAO calculation.

2.2.2 Cloud Brightness and Clear Sky Factor, K

The GOES imager data is used to calculate hourly estimates of cloud cover. This is a relatively simple method which uses an empirical relation that is roughly a linear relation between measured cloud brightness with K (Beyer et al., 1996). This has been shown to be valid in a number of studies.

Cloud brightness at time i , n_i is defined as:

$$n_i = \frac{V_i - \rho_i}{BX_i - \rho_i}$$

where V_i is the visible imager channel value, ρ_i is the surface albedo expressed in visible channel values, and BX_i is the maximum expected pixel brightness, also expressed in visible channel values. n_i ranges from 0 with no clouds, to 1

with complete cloud cover.

The surface albedo, ρ_i , is calculated for each pixel by taking the minimum measured value of V_i over the previous two weeks. This assumes that, at some point in that time frame, there were no clouds over that pixel. The maximum pixel brightness BX_i is calculated by taking the maximum value of *any* pixel for that time in the previous 14 days. To avoid single pixel anomalies, this value is taken on a 9x9 average of the visible image. This results in choosing bright pixels that are part of a large cloudy region.

Using these empirical methods for predicting ρ_i and BX_i avoids some confounding land surface effects. For example, differences due to changing solar view angles or seasonal changes in the surface are taken care of by the changing albedo values. The calculation of the clear sky factor from cloud brightness is almost 1 to 1:

$$k_i = \begin{cases} 1.2 & n_i > 1.2 \\ n_i & 0.2 < n_i < 1.2 \\ 5n_i^2/3 + n_i/3 + 1/15 & -0.1 < n_i < 0.2 \\ 0.05 & n_i < -0.1 \end{cases} \quad (12)$$

With hourly estimates of the clear sky factor, K_i , and the modeled clear sky solar radiation R_{soi} , the daily solar radiation is simply the sum of hourly products, $R_s = \sum_i K_i R_{soi}$. From this, a daily clear sky factor is calculated. This parameter is used to influence energy exchange with the atmosphere in the calculation of emitted longwave radiation. The daily clear sky factor, K is defined as $K = R_s/R_{so}$.

Figure 10 shows a comparison of the predicted and measured daily solar radiation at the CIMIS stations, from February 2003 through April 2006. The best fit correlation is nearly one-to-one when forcing the y-intercept through zero. Allowing the best fit y-intercept, shows some indication that GOES based estimates may over-predict radiation in low light levels, and under-predict radiation in very bright conditions. This could imply that the function mapping cloud brightness to a clear sky factor should be re-evaluated.

[Fig. 10 about here.]

The spatial distribution of errors for R_s is not equal over all parts of California as shown in Figure 4. The error is reported as the root mean squared error between the measurements and predictions. As can be seen, the areas along the coastline and some desert regions have the largest errors. Most of California shows significantly less difference between measured and predicted R_s .

[Fig. 11 about here.]

2.2.3 Net Longwave Radiation, R_{nl}

The daily net longwave radiation, R_{nl} , is derived from the Stefan-Boltzmann law, with an estimation of the net emissivity based on water vapor.

$$R_{nl} = -(1.35K - 0.35)(0.34 - 0.14\sqrt{e_a})\sigma \frac{(T_x + 273.16)^4 + (T_n + 273.16)^4}{2} \quad (13)$$

Most of these values are based on interpolated values with the exception of K . CIMIS estimates cloud cover as a ratio between the measured solar radiation

and predicted clear sky radiation; similar to the clear sky factor described in Section 2.2.2, but with a different clear sky radiation model. Figure 12 shows the difference between CIMIS R_{nl} and R_{nl} using GOES estimated K factors. As in the R_s comparison, the GOES method over-predicts R_{nl} in the cloudy regions and under-predicts in the clear regions. Why this is more pronounced in the R_{nl} comparison might be because of the difference in the calculation of the cloud factor, K . Since clear sky radiation is not a measured value at the CIMIS stations, it is unclear which estimation is more accurate.

[Fig. 12 about here.]

2.3 Winter Net Radiation Estimation Problems

Two winter phenomena in California adversely affected the net radiation predictions on certain occasions. These phenomena are snowfall and persistent fog, both common occurrences in California. Both problems lead to inaccurate estimations of surface albedo, which lead to inaccurate estimations of cloud cover, which lead to inaccurate estimations of net radiation. In the case of snowfall, the current method compares snowfall to the previous albedo and perceives freshly fallen snow as cloud cover, resulting in over predicting clouds and under predicting net radiation. In the case of persistent fog, a 14 day region of continuous fog will cause a large over prediction of albedo, and subsequently will under predict cloud cover and over predict net radiation for cloud covered regions.

A modification to the existing model, including adding additional GOES imager channels to differentiate between cloud and snow, and fog and surface is

being planned.

3 Measurement Uncertainty

The ET_0 model provides a single ET_0 value per pixel. To support the use of the output it is necessary to provide some information about the reliability of the predictions. For our model, interpolated data presents problems of under sampling and poorly distributed weather stations, while satellite imagery presents problems with the method of retrieval and derivation used.

To estimate uncertainty, Monte Carlo simulations are run on the daily estimations. Normally distributed errors are associated with each input parameter to the ET_0 calculation, for each pixel in the image. Because of the proximity of CIMIS stations, elevation differences, and other spatially varying considerations, the errors for each parameter vary across the image. Table 3 summarizes the standard deviation used for each parameter. Here, the difference of the two estimations for temperatures are used to set error bounds on T_n , T_x , T_{dewp} , and, indirectly, e_a and e_s . The radiation parameter errors are modeled as percentages of the radiation values. R_s , especially, has a higher error than the comparison to the CIMIS data suggest, but was increased to simulate differences in calculations of R_{so} as mentioned in Section 2.2. Wind speed, U_2 , errors were estimated.

[Table 3 about here.]

For each day, standard deviation maps are computed for every parameter. For each parameter, an image of random Gaussian distributed errors with mean 0 and standard deviation 1 is calculated and multiplied with the parameter's

standard deviation map. The resultant errors are added to the estimated values for each parameter, and ET_0 is calculated. This is carried out for a number of error maps. The variance of the calculated ET_0 estimations can then be used as an estimate to the error associated with the ET_0 prediction.

Because of computing limitations, only 10 separate Monte-Carlo runs are performed per day. This number is low enough that the resultant maps of predicted error in the ET_0 calculations shows randomization patterns and are speckled. To improve the output, the error map is run through a 3x3 averaging filter. In a sense, this creates a pseudo error map of 90 Monte-Carlo runs, and eliminates the random patterns.

Figure 13 shows the average error estimates of uncertainty for ET_0 as isolines on the average ET_0 values. This is for the month of August, 2005.

[Fig. 13 about here.]

Uncertainty analysis is run every day to estimate spatial uncertainty of the results. However, these estimates can be misleading in certain cases, for example, the error estimation for the temperature parameters assumes there is no bias in the two interpolation methods. This has not been validated.

4 Conclusions

ET is an important indicator in both agricultural and urban settings and can address water needs for a variety of water issues, such as irrigation scheduling.

We have demonstrated a method of creating daily ET_0 maps for California using satellite and ground station data. The current method provides good

estimates of ET_0 and will be incorporated in the California Irrigation Management Information System program, providing users access to spatial distributions of ET_0 . The model has been used with GOES and CIMIS data for approximately three years, since February, 2003.

Net radiation models combined with GOES estimates of cloud cover is an effective method of obtaining spatial estimations of solar radiation. Some events like snowfall and persistent fog, lead to erroneous cloud cover predictions. Including additional GOES channels to detect these events is an important next step.

Variations in the temperature distributions throughout California are caused by multiple forces and can be difficult to model completely with interpolation methods alone, especially in regions where stations are sparse. One possibility being investigated will use weather prediction models, run at small time scales, and periodically modified by near real-time hourly data from weather stations to more accurately model the spatial variability of surface parameters.

Monte-Carlo methods can be used on spatial calculations to understand more accurately what the impact of uncertainties in parameter estimations can have on final model outputs.

References

- Allen, R. G., Pereira, L. S., Raes, D., Smith, M., 1998. Crop evapotranspiration : guidelines for computing crop water requirements. FAO irrigation and drainage paper 56, Food and Agriculture Organization of the United Nations, Rome.

URL <http://www.fao.org/docrep/X0490E/x0490e00.htm>

Beyer, H., Costanzo, C., Heinmann, D., 1996. Modifications of the Heliosat procedure for irradiance estimates from satellite images. *Solar Energy* 56 (3), 207–212.

GRASS Development Team, 2006. Geographic Resources Analysis Support System (GRASS GIS) Software. ITC-irst, Trento, Italy.

URL <http://grass.itc.it>

Leferve, M., Aluisson, M., Wald, L., November 2002. Description of the software Heliosat-II for the conversion of images acquired by meteosat satellites in the visible band into maps of solar radiation available at ground level. Tech. rep., Ecole Des Mines De Paris.

URL <http://www.heliolim.org/heliosat>

Mitasova, H., Mitas, L., Brown, W., Gerdes, D., Kosinovsky, I., Baker, T., 1995. Modeling spatially and temporally distributed phenomena: new methods and tools for GRASS GIS. *International Journal of Geographical Information Systems* 9(4), 433–446.

Neteler, M., Mitasova, H., 2004. Open Source GIS: A GRASS GIS Approach, 2nd Edition. Springer, Boston.

Peter E. Thornton, S. W. R., White, M. A., March 1997. Generating surfaces of daily meteorological variables over large regions of complex terrain. *Journal of Hydrology* 190, 214–251.

Remund, J., Wald, L., Lefevre, M., Ranchin, T., Page, J., June 2003. Worldwide linke turbidity information. In: Proceedings of ISES Solar World Congress. Gteborg, Sweden.

URL http://www.helioclim.net/publications/isesh2003_linke.pdf

Rigollier, C., Bauer, O., Wald, L., 2000. On the clear sky model of ESRA – European Solar Radiation Atlas – with respect to the heliosat method. *Solar*

Energy 68 (1), 33–48.

Walter, I., Allen, R., Elliott, R., Jensen, M., Howell, T., Snyder, R., Brown, P., Echings, S., Spofford, T., Wright, J., June 2000. ASCE's standardized reference evapotranspiration equation. In: American Society Of Civil Engineers Watershed Management Conference. p. 11.

List of Figures

1	ET_0 estimations on 2005/06/18. The scale is in mm day ⁻¹ .	23
2	Processing steps for generating ET_0 . The left side shows the integration of hourly GOES imagery to estimate radiation parameters. The right side shows weather station interpolations usually with two procedures.	24
3	CIMIS weather stations. Larger symbols imply higher elevations.	25
4	Histograms of elevations for California from a (2 km) ² digital elevation model and CIMIS stations.	26
5	Regularized Spline with Tension (RST) interpolations from air temperatures on 2005/06/18 normalized to sea level, and the air temperature estimates after correcting for elevation. The method predicts gradual changes in the normalized temperature, while maintaining strong elevation dependence of the temperature values.	27
6	Lapse rate measurements for three regions of California, for T_x, T_n and T_{dewp} .	28
7	Example of temperature interpolation comparing the TG method and RST for one day, 2005/06/18.	29
8	Two typical wind speed interpolations, for a calm and a windy day.	30
9	Solar radiation calculations are performed on zenith intervals, using hourly cloud cover estimates.	31
10	A comparison of measured vs. GOES estimated radiation, for all CIMIS stations over about 3 years.	32
11	Percent difference between the CIMIS measurements and GOES estimations of R_s for California.	33
12	GOES based estimates of net longwave radiation compared to CIMIS ground station estimates.	34
13	Estimated ET_0 error for 2005-08. Raster colors indicate estimated ET_0 , and isolines show error estimates with labels in mm.	35

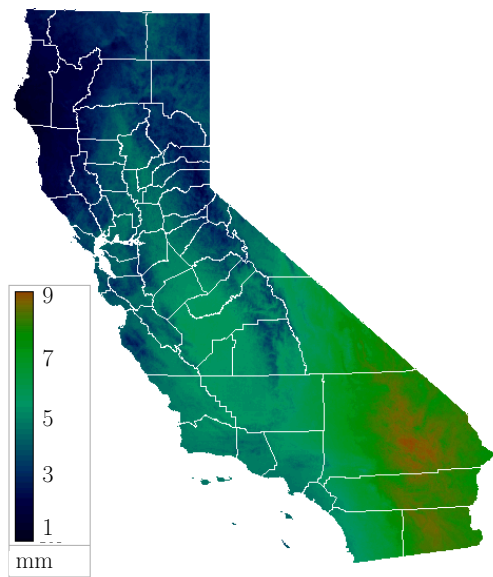


Fig. 1. ET_0 estimations on 2005/06/18. The scale is in mm day^{-1} .

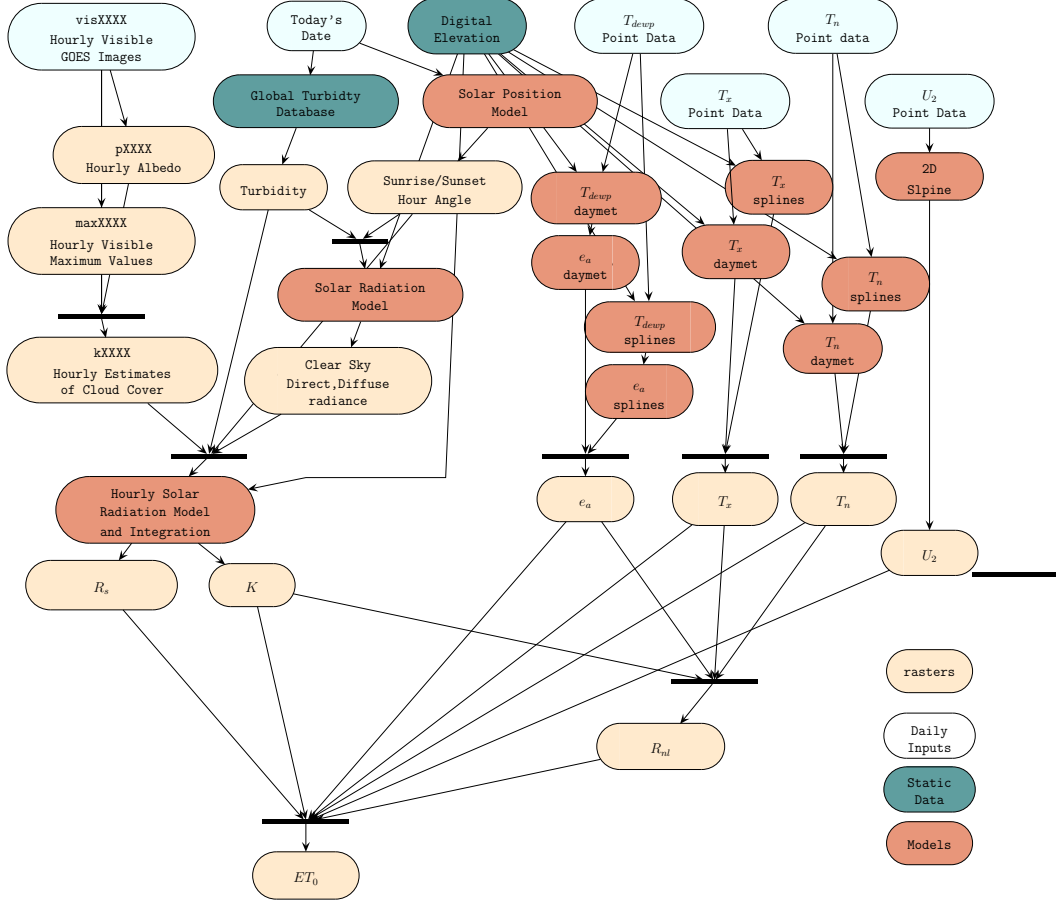


Fig. 2. Processing steps for generating ET_0 . The left side shows the integration of hourly GOES imagery to estimate radiation parameters. The right side shows weather station interpolations usually with two procedures.

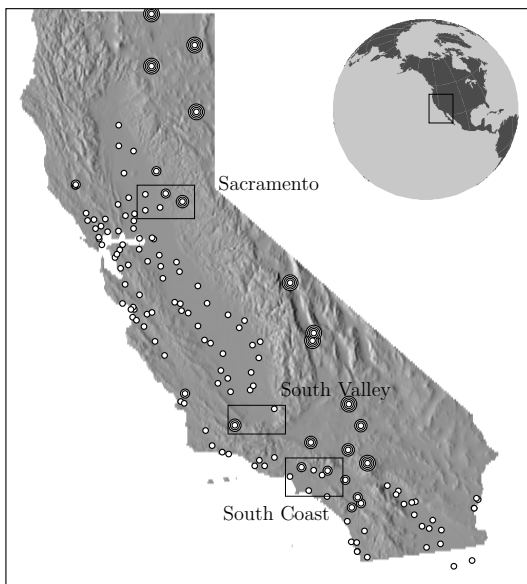


Fig. 3. CIMIS weather stations. Larger symbols imply higher elevations.

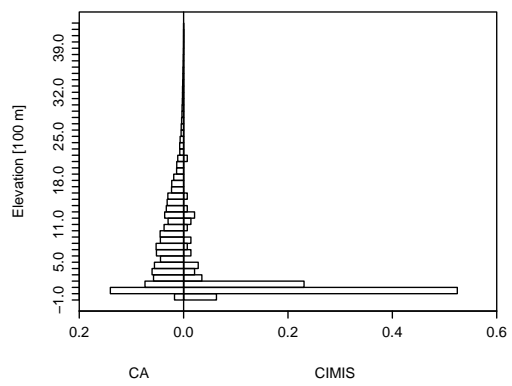


Fig. 4. Histograms of elevations for California from a $(2 \text{ km})^2$ digital elevation model and CIMIS stations.

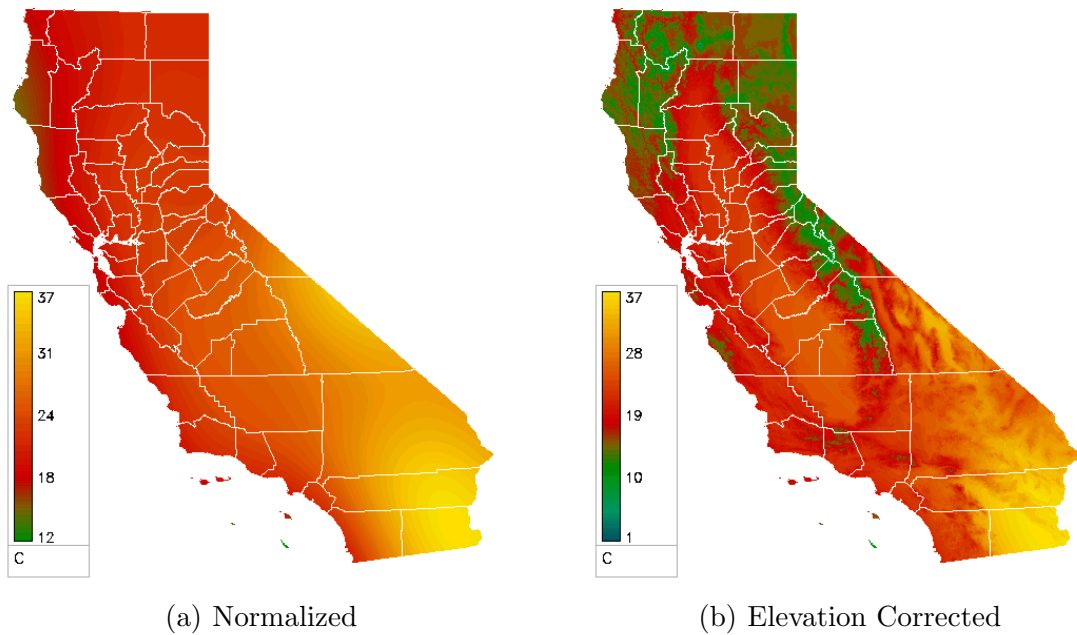


Fig. 5. Regularized Spline with Tension (RST) interpolations from air temperatures on 2005/06/18 normalized to sea level, and the air temperature estimates after correcting for elevation. The method predicts gradual changes in the normalized temperature, while maintaining strong elevation dependence of the temperature values.

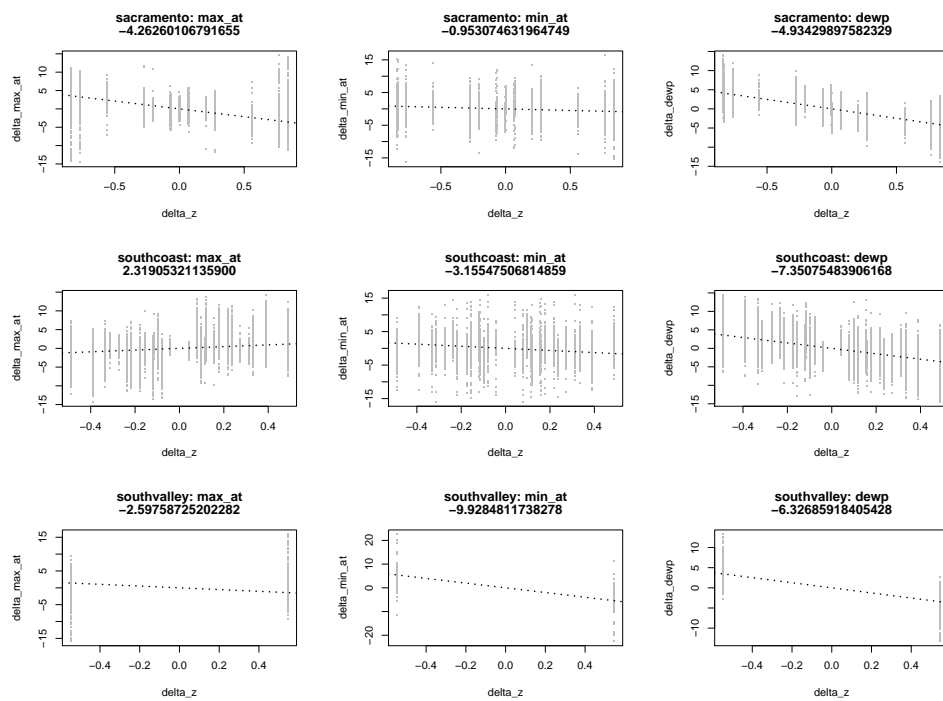


Fig. 6. Lapse rate measurements for three regions of California, for T_x, T_n and T_{dewp} .

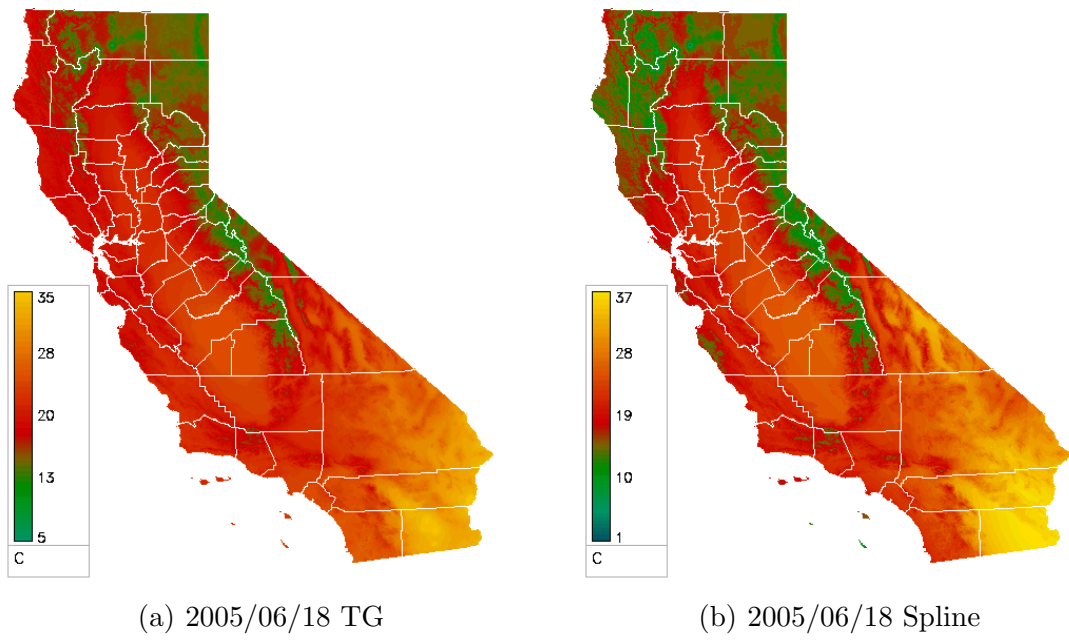


Fig. 7. Example of temperature interpolation comparing the TG method and RST for one day, 2005/06/18.

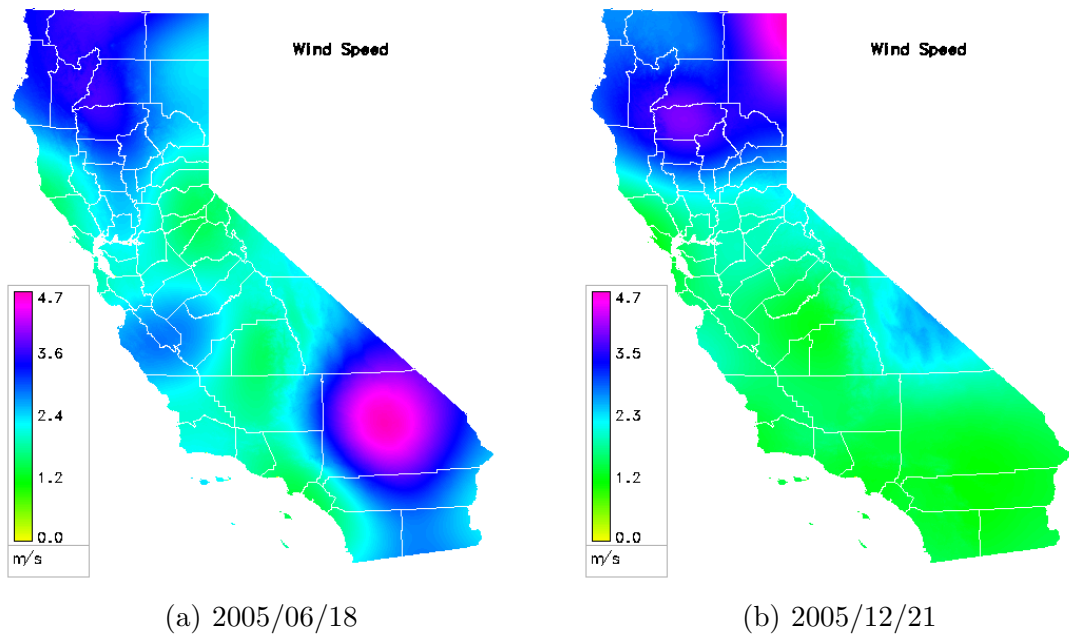


Fig. 8. Two typical wind speed interpolations, for a calm and a windy day.

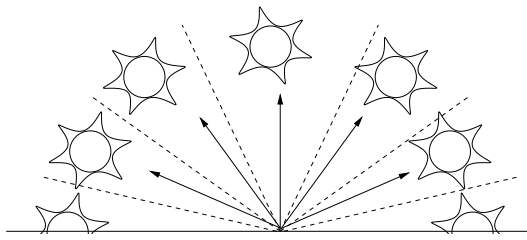


Fig. 9. Solar radiation calculations are performed on zenith intervals, using hourly cloud cover estimates.

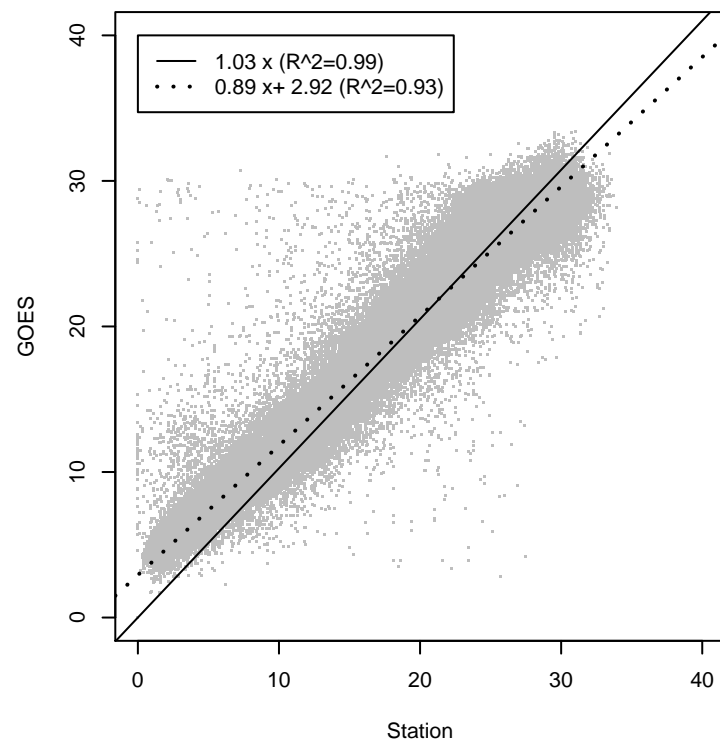


Fig. 10. A comparison of measured vs. GOES estimated radiation, for all CIMIS stations over about 3 years.

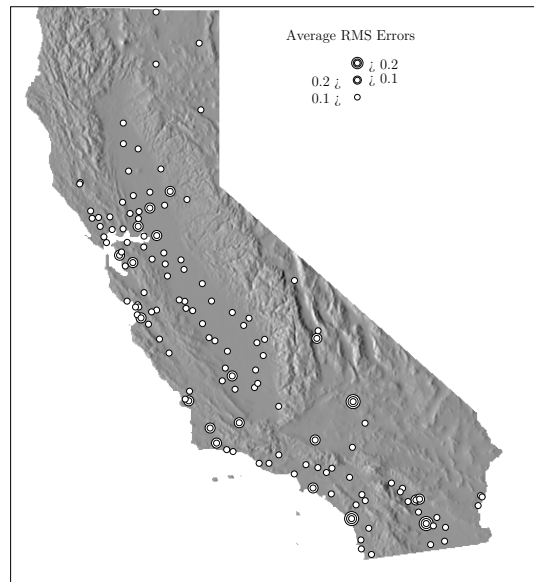


Fig. 11. Percent difference between the CIMIS measurements and GOES estimations of R_s for California.

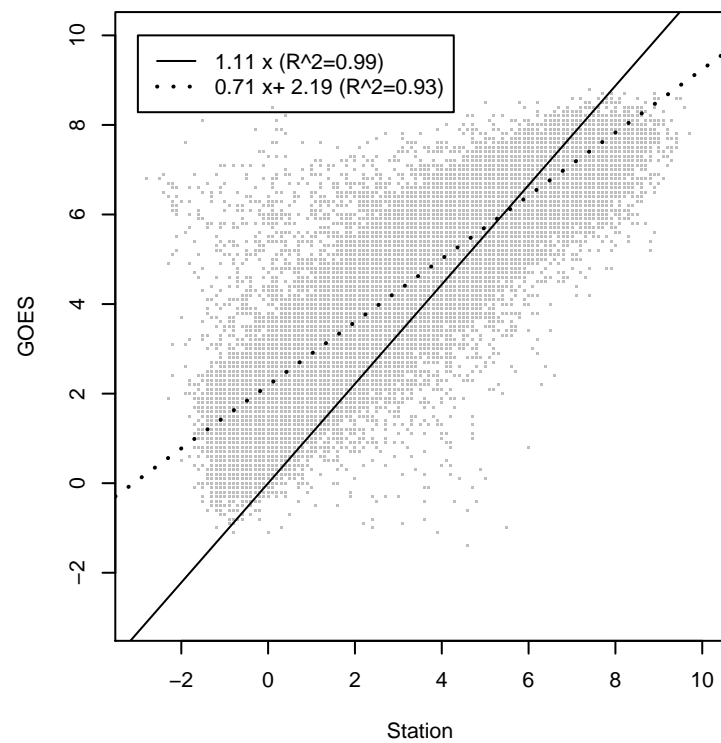


Fig. 12. GOES based estimates of net longwave radiation compared to CIMIS ground station estimates.

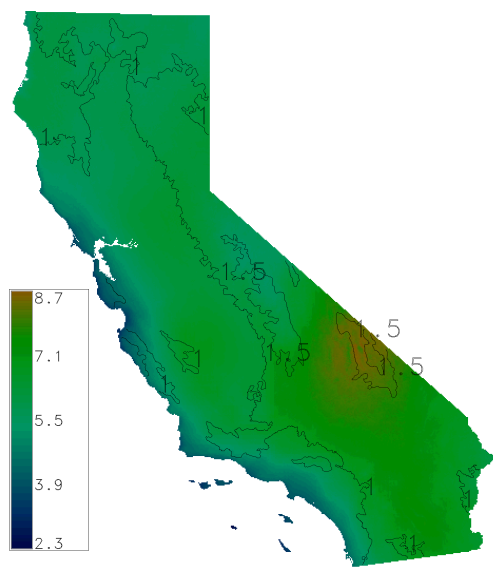


Fig. 13. Estimated ET_0 error for 2005-08. Raster colors indicate estimated ET_0 , and isolines show error estimates with labels in mm.

List of Tables

1	Symbols used in this report	37
2	Average monthly surface temperature lapse rate measurements [°C/km] for various California transects.	38
3	Error contributions	39

Table 1
Symbols used in this report

Symbol	Description	Units
ET	Evapotranspiration	mm/day
ET_0	reference evapotranspiration	mm/day
R_n	net radiation	MJ/m ² day
R_{nl}	net longwave radiation	MJ/m ² day
R_s	solar radiation	MJ/m ² day
R_{so}	clear sky solar radiation	MJ/m ² day
G	soil heat flux density	MJ/m ² day
α_a	mean air density at constant pressure	kg/m ³
c_p	specific heat of air	MJ/kg °C
r_a	aerodynamic resistance	s/m
r_s	bulk surface resistance	s/m
T_m	daily mean air temperature at 1.5 m height	°C
T_n	daily minimum air temperature at 1.5 m height	°C
T_x	daily maximum air temperature at 1.5 m height	°C
T_{dewp}	dew point temperature at 1.5 m height	°C
U_2	wind speed at 2 m height	m/s
Rh_{max}	maximum relative humidity	%
e_a	actual vapor pressure	kPa
e_s	saturation vapor pressure	kPa
γ	psychrometric constant	kPa/°C
Δ	slope of vapor pressure-temperature curve	kPa/°C
K	clear sky factor	
σ	Stefan-Boltzmann constant = $4.903e^{-9}$	MJ/m ² K ⁴ day
α	Albedo	

Table 2

Average monthly surface temperature lapse rate measurements [$^{\circ}\text{C}/\text{km}$] for various California transects.

Month	South Coast			South Valley			Sacramento		
	T_x	T_n	T_{dewp}	T_x	T_n	T_{dewp}	T_x	T_n	T_{dewp}
Jan	-3.34	-3.81	-9.44	3.25	-7.29	-7.66	0.20	-1.93	-4.93
Feb	-3.13	-3.68	-10.22	-3.93	-7.50	-6.48	-4.50	-2.29	-5.62
Mar	0.46	-3.94	-7.58	-4.73	-10.39	-6.14	-5.54	-2.49	-5.49
Apr	-0.46	-3.97	-6.42	-4.67	-10.18	-5.59	-6.50	-2.84	-3.83
May	4.15	-3.09	-6.52	-3.79	-10.69	-5.65	-6.48	-2.43	-3.58
Jun	6.63	-5.31	-3.76	-3.63	-12.83	-5.09	-5.47	-1.27	-3.33
Jul	10.36	-2.38	-4.63	-2.91	-13.02	-6.46	-3.53	2.67	-4.94
Aug	9.99	-2.02	-6.04	-3.23	-12.51	-5.45	-3.09	2.38	-6.50
Sep	6.22	-0.80	-7.30	-3.17	-11.39	-5.39	-4.08	0.81	-6.97
Oct	1.56	-1.68	-5.74	-3.53	-8.34	-6.69	-4.68	-0.33	-5.27
Nov	-2.20	-3.64	-9.45	-0.94	-6.87	-8.38	-2.64	-0.55	-4.56
Dec	-3.05	-3.23	-11.06	1.62	-5.71	-8.43	-2.33	-1.74	-4.28

Table 3
Error contributions

Parameter	Std. Dev.	Description
T_x	$\sqrt{2} \Delta(T_x) $	$\Delta(T_x)$ is difference in interpolations
T_n	$\sqrt{2} \Delta(T_n) $	$\Delta(T_n)$ is difference in interpolations
T_{dewp}	$\sqrt{2} \Delta(T_{dewp}) $	$\Delta(T_{dewp})$ is difference in interpolations
e_a	$\sqrt{2} \Delta(e_s) $	$\Delta(e_a)$ is difference in interpolations
R_s	$0.15*R_s$	Estimated from different R_s calculations
R_{nl}	$0.15*R_{nl}$	Estimated from different R_{nl} calculations
U_2	$0.25*U_2$	Estimated